

ADAPTIVE OPTICS OBSERVATIONS OF B0128+437: A LOW-MASS, HIGH-REDSHIFT GRAVITATIONAL LENS

DAVID J. LAGATTUTA¹, MATTHEW W. AUGER², AND CHRISTOPHER D. FASSNACHT¹

Received 2009 December 11; accepted 2010 May 19

ABSTRACT

We use high-resolution adaptive optics (AO) imaging on the Keck II telescope to study the gravitational lens B0128+437 in unprecedented detail, allowing us to resolve individual lensed quasar components and, for the first time, detect and measure properties of the lensing galaxy. B0128+437 is a small separation lens with known flux-ratio and astrometric anomalies. We discuss possible causes for these anomalies, including the presence of substructure in the lensing galaxy, propagation effects due to dust and a turbulent interstellar medium, and gravitational microlensing. This work demonstrates that AO will be an essential tool for studying the many new small-separation lenses expected from future surveys.

Subject headings: galaxies: high-redshift — galaxies: individual (CLASS B0128+437) — gravitational lensing: strong — infrared: galaxies

1. INTRODUCTION

Galaxies acting as strong gravitational lenses can provide important insights into the distribution of matter on small scales, as the brightness and position of the multiple lensed images are directly related to the gravitational potential of the foreground galaxy. Many lenses are well modeled by a smooth potential. For other lenses, however, a simple mass model is incapable of accurately predicting the positions of the multiple images of the background object (astrometric anomalies), or the relative brightness between image pairs (flux-ratio anomalies). The existence of these astrometric and flux-ratio anomalies in lenses has been used to study the presence of galactic substructure (Dalal & Kochanek 2002; Xu et al. 2009) – predicted by numerical simulations of the Λ CDM theory of structure formation (Diemand et al. 2008; Springel et al. 2008) – as well as propagation effects such as dust extinction and scatter broadening.

In this letter we discuss one such anomalous lens, CLASS B0128+437 (Phillips et al. 2000). First observed as part of the Cosmic Lens All-Sky Survey (e.g., Myers et al. 2003; Browne et al. 2003), B0128+437 is a compact four-image system with a maximum image separation of $0.54''$. Very Long Baseline Interferometry (VLBI) imaging presented by Biggs et al. (2004; B04) revealed three distinct subcomponents in each of the lensed source images. Lens modeling in B04 could not sufficiently reproduce either the positions of these subcomponents in images B and C or the total flux of image B, suggesting that some form of substructure was present in the lens system.

McKean et al. (2004) determined a redshift of $z_s = 3.124$ for the source galaxy, and an emission line not associated with the source was posited to be either H α (implying a lens redshift $z_l = 0.218$), H β ($z_l = 0.645$), or [O II] ($z_l = 1.145$). Their analysis suggested that [O II]

was the most likely candidate; if confirmed, this would indicate that B0128+437 is the most distant known gravitational lens.

Given the small image separation and a possible [O II] emission line, the lensing galaxy in the B0128+437 system may be a late-type galaxy. Ground based images in the infrared (IR) from UKIRT (B04) have not been able to resolve the system, and space based images in the IR (NICMOS; Biggs 2004; Figure 1, left) and optical (WFPC2) have had neither the resolution nor, in the case of WFPC2, sufficient sensitivity to investigate the properties of the system.

In this Letter we present a different method of observing B0128+437: ground-based near-IR imaging coupled with laser guide-star adaptive optics (LGS AO). While AO imaging has been used on gravitational lenses in the past (Crampton et al. 1998; Marshall et al. 2007; McKean et al. 2007; Auger et al. 2008), the systems studied have been high-mass lenses producing image separations of $\sim 2''$. With B0128+437, we present the first results of using AO with a small-separation gravitational lens, demonstrating that AO imaging is capable of probing the details of low-mass systems.

Throughout this Letter, we assume a concordance cosmological model, with $\Omega_M = 0.3$, $\Omega_\Lambda = 0.7$, and a Hubble parameter $H_0 = 70 h_{70} \text{ km s}^{-1} \text{ Mpc}^{-1}$. All magnitudes presented are AB magnitudes.

2. OBSERVATIONS

We observed the B0128+437 system using the Near Infrared Camera 2 (NIRC2; K. Matthews et al., in preparation) on the Keck II telescope along with the the LGS AO system, under photometric conditions, on UT 2009 September 12. We used the narrow camera ($10'' \times 10''$ field of view, $0.01''/\text{pixel}$ scale) to properly sample the diffraction-limited core of the point-spread function (PSF). The data were obtained using the Kp filter and were dithered to mitigate the effects of bad pixels, cosmic ray strikes, and detector persistence. Each exposure was 180 seconds to stay within the linear regime of the detector and to minimize the variation in sky brightness for flat-fielding. After visually inspecting cleaned indi-

lagattuta@physics.ucdavis.edu

¹Department of Physics, University of California, Davis, 1 Shields Avenue, Davis CA 95616

²Department of Physics, University of California, Santa Barbara, CA 93106

Table 1
Lens System Parameters

Component	Kp	$\Delta\alpha(^{\prime\prime})^a$	$\Delta\delta(^{\prime\prime})^a$
Image A	21.55 ± 0.03	$\equiv 0.0$	$\equiv 0.0$
Image B	23.49 ± 0.22	0.099	0.095
Image C	22.49 ± 0.04	0.521	-0.170
Image D	22.87 ± 0.12	0.109	-0.260
Lens galaxy (total)	20.99 ± 0.08	0.217	-0.104
Lens galaxy(R_{Ein}) ^b	22.15 ± 0.10	0.217	-0.104

^a Uncertainties are ~ 0.001 for B/C/D and ~ 0.01 for the galaxy.

^b Aperture magnitude with $R = R_{\text{Ein}} = 0.24''$.

vidual exposures and rejecting frames where the image appeared strongly distorted due to loss of LGS lock or problems with the AO wavefront sensors, we were left with 30 frames and a total exposure time of 5400 s.

The data were reduced using the Center for Adaptive Optics Treasure Survey (CATS)³ NIRC2 pipeline, modified to properly correct for the geometric distortion of the narrow camera⁴. The reduced image frames were then stacked using the Drizzle routine (Fruchter & Hook 2002) in IRAF, using sub-pixel offsets determined via cross-correlation.

The results of the reduction can be seen in the middle panel of Figure 1. We see the four lensed quasar images clearly, along with the lensing galaxy and a partial Einstein ring from the quasar host galaxy. This is a significant improvement over the 5440 s NICMOS F160W image.

3. MODELING MASS AND LIGHT

We are primarily interested in the light of the lensing galaxy and any substructure that might be associated with it and we therefore treat the lensed quasar and its host galaxy (the Einstein ring) as nuisances. We model the flux in the image as various components: a Sérsic profile (Sérsic 1963) for the lensing galaxy, PSF models for the quasi-stellar object (QSO) images, and a lensed Sérsic profile for the QSO host galaxy. We then marginalize over the parameters of the source components to infer the properties of the lensing galaxy. Note that we do not treat the QSO images as being lensed; this is because we suspect that simple lens models will not be sufficient to reproduce the observed fluxes, complicating our attempts to model the light. We do not use the QSO image positions to constrain the lens model, because we are able to obtain a robust subtraction of the Einstein ring by using the data in the ring itself and assuming the Singular Isothermal Ellipsoid (SIE) + external shear parameters from B04 as a starting point for the lens model; the final model is consistent with the B04 model, given the uncertainties. It is interesting that we are able to sufficiently remove the Einstein ring flux with a simple model, as it implies that the known anomalies present in the B0128+437 system are not the result of incorrect assumptions about the global mass model, but rather due to some localized discrepancy (§4.2).

The PSF model is determined from the data by fitting a model of three Gaussian components to the QSO images; one component represents the diffraction-limited

core, another represents the seeing-limited diffuse PSF, and the third encodes structure in the PSF, as seen in the C and D components in Figure 1 (middle). The full model (Sérsic lens, four QSO PSFs, and lensed QSO host) is fit to the data iteratively, using a Levenberg-Marquardt optimization algorithm to find the minimum in the parameter space. A set of Markov Chain Monte Carlo simulations are run to probe the parameter space around this minimum and obtain uncertainty estimates for the quasar image fluxes, lens flux, and lens position. The results of the modeling are shown in Figure 1 (right) and the best-fit parameters for the lensing galaxy and QSO positions and fluxes are tabulated in Table 1.

4. DISCUSSION

The improved image resolution provided by the AO data allows us to (1) for the first time observationally detect the lensing galaxy and estimate its light profile, (2) measure flux ratios between pairs of lensed images without worrying about blending effects, and (3) search for luminous substructure.

4.1. The Lens Galaxy

In the rightmost panel of Figure 1 we clearly see the B0128+437 lens galaxy. We measure a total magnitude of $Kp = 20.99 \pm 0.08$. Using the B04 model Einstein radius $R_{\text{Ein}} = 0.24''$, we further measure an Einstein radius aperture magnitude $Kp_{\text{Ein}} = 22.15 \pm 0.10$. We are unable to obtain robust constraints on either the effective radius or the Sérsic index, although we note that in all iterations of our modeling, the Sérsic index lies between $n = 1$ and $n = 2.5$, which suggests either a lenticular or late-type galaxy morphology.

We use Maraston (2005; M05) instantaneous burst stellar population models with solar metallicity to infer the age of the lens galaxy stellar population. We use models with predominantly stellar lensing mass (i.e., a stellar fraction $f_* \sim 1$) within the Einstein radius, which are consistent with the results for low-mass S0 galaxies from Tortora et al. (2009) and with previous results from lenses (Auger et al. 2009) after extrapolating to the mass of B0128+437. We then infer the observed Kp-band magnitude for each of the candidate lens redshifts from the M05 models for a range of stellar population ages and compare this in a χ^2 sense with the observed magnitude within the Einstein radius (Figure 2). For redshift $z_l = 0.218$, no acceptable solution – i.e. one in which the stellar age was less than the age of the universe – is found unless we assume an unusually low ($f_* = 0.3$) stellar fraction. This analysis does not strongly favor either of the other two proposed lens redshifts, $z = 1.145$ and $z = 0.645$, both of which give stellar ages that are less than the age of the universe for reasonable values of f_* . However, after combining this with the previous photometric and spectroscopic data, we continue to slightly favor the higher redshift $z = 1.145$. The inferred age for $z = 1.145$ is ~ 3.2 Gyr (Table 2) and the rest-frame K-band luminosity inferred from the M05 model is $\log_{10}(L_{K,\text{Ein}}) = 10.61 L_{\odot}$ (the age and luminosity for $f_* = 0.9$ are 2.7 Gyr and $\log_{10}(L_{K,\text{Ein}}) = 10.67 L_{\odot}$). This results in a mass-to-light ratio $M/L_{K,\text{Ein}} = 0.68$ which is, by construction, consistent with a stellar population that formed ~ 3 Gyr ago.

³ <http://irlab.astro.ucla.edu/cats/index.shtml>

⁴ <http://www.astro.caltech.edu/~pbc/AO/distortion.pdf>

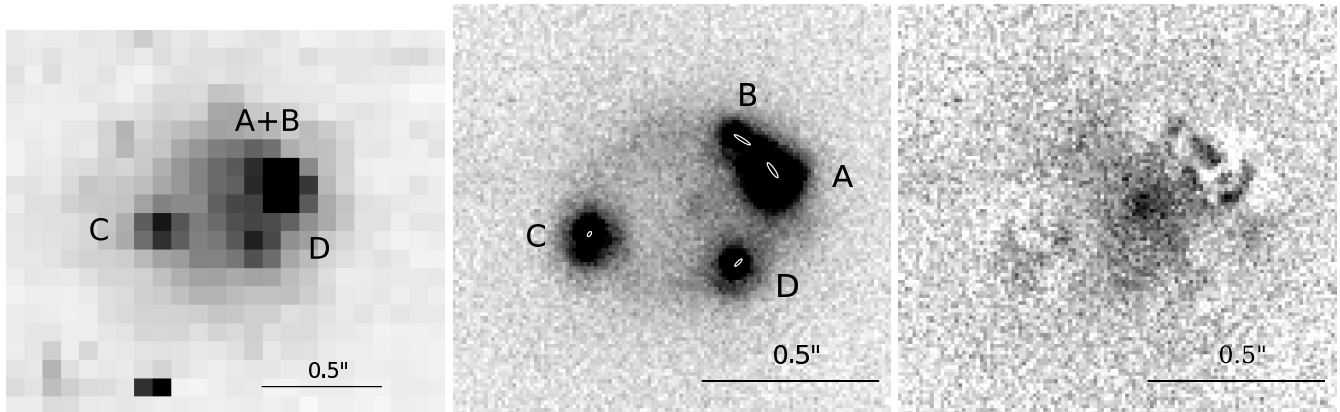


Figure 1. **Left:** NICMOS F160W image of B0128+437. The resolution of HST in this band makes it difficult to resolve individual components. **Middle:** AO image of B0128+437. The four lensed quasar images [A–D] are clearly seen and easily resolved, along with a partial Einstein ring from the quasar host galaxy. The $3\text{-}\sigma$ 2.3 GHz contours of B04 are overlaid in white. Additionally, the lensing galaxy can be seen lying close to A, B, and D in the image plane. **Right:** Flux remaining in the B0128+437 system after subtracting the source quasar and host galaxy light. The lens galaxy is now clearly visible. Note that the image stretch in this panel is different from that of the middle panel.

Table 2
Redshift Dependent Lens Galaxy Properties

z_l	Stellar Age ^a (h_{70}^{-1} Gyr)	$\log_{10} L_{K,\text{lens}}$ ($h_{70}^{-2} L_{\odot}$)	$\log_{10} L_{K,\text{Ein}}$ ($h_{70}^{-2} L_{\odot}$)	$\log_{10} M_{\text{Ein}}^b$ ($h_{70}^{-1} M_{\odot}$)	$M/L_{K,\text{Ein}}$ ($h_{70} M_{\odot}/L_{\odot}$)	σ_{SIE}^b (km s^{-1})
0.218	10.8	9.53 ± 0.03	9.07 ± 0.04	9.78	5.13 ± 0.04	98
0.645	8.5	10.55 ± 0.04	10.09 ± 0.04	10.20	1.29 ± 0.04	114
1.145	3.2	11.07 ± 0.05	10.61 ± 0.05	10.44	0.68 ± 0.05	138

^a Measured assuming a stellar fraction $f_* = 1.0$ for $z_l = \{0.645, 1.145\}$ and $f_* = 0.3$ for $z_l = 0.218$.

^b Determined using the B04 mass model with $R_{\text{Ein}} = 0.24''$.

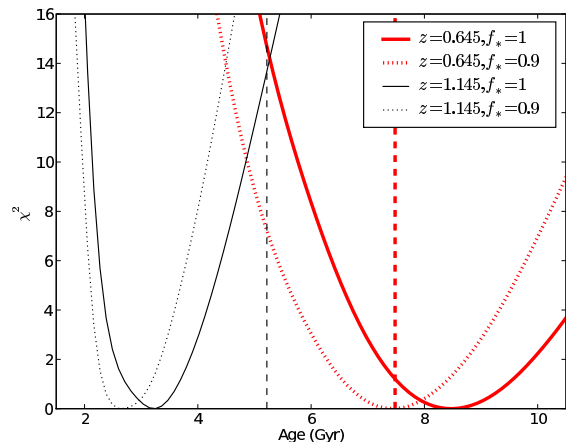


Figure 2. Inference on the stellar age of the lensing galaxy by comparing the observed magnitude (Kp = 22.15) with M05 models of varying ages. The solid (dotted) curves represent a stellar fraction $f_* = 1$ ($f_* = 0.9$), while the vertical dashed lines denote the age of the universe at the assumed lens redshift. The two sets of curves represent lens redshifts of $z_l = 1.145$ (black) and $z_l = 0.645$ (red); the lens redshift $z_l = 0.218$ leads to stellar population ages older than the age of the universe at that redshift for $f_* > 0.3$.

4.2. Flux Ratios

Our models give accurate fluxes for each image separately, allowing us to calculate flux ratios. We present these flux ratios, along with the radio flux ratios of B04, in Table 3. While there is significant variation between the flux ratios in different bands, one feature that per-

Table 3
Multi-band Flux-ratio Data

Flux Ratio	Kp	X	C	S	L
f_B/f_A	0.17 ± 0.03	...	0.56	0.49	...
f_C/f_A	0.42 ± 0.01	...	0.49	0.34	...
f_D/f_A	0.30 ± 0.03	...	0.47	0.47	...
f_C/f_D	1.43 ± 0.16	0.67	1.04	0.72	0.75

Flux ratios between image pairs. We present Kp flux ratios, along with previously measured flux ratios in the X (3.5 cm), C (6 cm), S (13 cm), and L (21 cm) radio bands. In the X and L bands, only images C and D are sufficiently deblended to measure accurate flux ratios. Due to the extreme blending of flux between images, flux ratios measured in the F160W NICMOS image are unreliable, and thus not included. All radio data are taken from B04, with errors $\lesssim 5\%$.

sists in both the radio and near-IR regimes is the unusual value of f_B/f_A . The close proximity of A and B suggests that they should have nearly the same flux and a negligible time delay (e.g., Keeton et al. 2005); the discrepancy between what is seen in the data and what is expected from smooth mass models therefore cannot be due to intrinsic variability in the source. We therefore discuss several other phenomena that may contribute to the flux-ratio anomaly.

4.2.1. Substructure

Substructure, in the form of satellite galaxies and dark matter clumps associated with the lensing galaxy,

could explain the anomalous f_B/f_A , especially since some lenses with flux-ratio anomalies are known to have luminous satellites whose presence can account for the anomalies (e.g., MG0414+0534: Ros et al. 2000; MG2016+112: More et al. 2009; B2045+265: McKean et al. 2007). This scenario is appealing because VLBI imaging of B0128+437 shows astrometric anomalies of the quasar image positions. The presence of substructure perturbs the gravitational potential and consequently alters the position *and* the brightness of the lensed images; substructure could therefore be responsible for both anomalies.

However, since lensing is an achromatic effect, the measured flux ratios in the radio regime should be the same as those measured in the near-IR. Instead, the near-IR f_B/f_A is significantly smaller than its radio wavelength counterparts (Table 3). Therefore, it seems unlikely that substructure alone is responsible for the anomaly.

Furthermore, after subtracting both the source and lens flux, we find no obvious luminous substructure in the vicinity of B0128+437; the flux that remains in the right panel of Figure 1 is most likely an artifact of model subtraction. However, the fact that we do not directly detect luminous substructure may not be surprising. B04 estimate that a perturbing mass as low as $10^6 M_\odot$ could account for the milliarcsecond-scale astrometric discrepancies observed in B0128+437. If we assume reasonable M/L ratios for such an object, it falls well below our detection threshold.

We determine a limiting magnitude for our imaging by populating the image with randomly placed simulated point sources covering a range of magnitudes from $K_p = 23.5$ to $K_p = 28.5$. We then analyze these images with SExtractor (Bertin & Arnouts 1996) and find that we can repeatedly recover sources as faint as $K_p = 25.5$, which we take to be our detection limit. This corresponds to a rest-frame V band luminosity $M_V = -17$, comparable to the Magellanic Clouds. We note, however, that the detection limit is significantly brighter very close to the lensed images due to the increased shot noise from the quasars.

4.2.2. Propagation Effects

Propagation effects can also account for the f_B/f_A anomaly, with scatter broadening by the lensing galaxy interstellar medium affecting the radio fluxes and dust extinction affecting the near-IR fluxes, giving rise to the chromatic nature of the flux-ratio anomaly. If dust were solely responsible for the near-IR anomaly, image B would need to be dimmed by ~ 2.0 magnitudes of extinction (assuming as a lower limit that image A is not being affected). Using the Calzetti et al. (2000) reddening law for rest-frame J-band, this corresponds to an $E(B-V)$ value of 1.01, equivalent to ~ 4.1 magnitudes of rest-frame V-band extinction. While this is large, it is not unphysical: studies of the local group have revealed pockets of dust in nearby giant molecular clouds (GMCs) that cause up to 10 V-band magnitudes of extinction (Cambr esy 1999).

In the radio, scatter broadening by a GMC may explain why image B shows a decrease in surface brightness and why its subcomponents seen in 5 GHz VLBI imaging are much broader than those of other images. This scenario has been postulated for the grav-

itational lens B0218+357, where a GMC is thought to be responsible for the broadening/dimming of image A (Grundahl & Hjorth 1995; Zeiger & Darling 2010).

However, while this explains the flux-ratio anomaly, known GMCs are not massive enough to significantly alter the lensing potential and cause the astrometric anomalies shown by images B and C. Therefore, it is unlikely that propagation effects alone can explain all of the observed properties.

4.2.3. Microlensing

A third phenomenon that could explain the f_B/f_A flux-ratio anomaly is extragalactic microlensing, where small gravitational distortions due to stars in the lensing galaxy affect the fluxes of images (e.g., Wambsgans 2006). While the size of the radio-emitting regions of active galaxies are often too large to be significantly affected by the lensing cross section of individual stars, microlensing of the accretion disk (the source of the near-IR emission in B0128+437) can substantially change the observed flux of a given image. Microlensing could, therefore, explain the discrepant flux ratios between the radio and near-IR data.

However, while it is possible to observe some microlensing in radio bands, the flux discrepancies measured for other lens systems are much less dramatic than the radio f_B/f_A values of B0128+437. Studies involving B1608+656: (Fassnacht et al. 2002) and B1600+434: (Koopmans & de Bruyn 2000) show only small ($\sim 3\%$) microlensing radio flux-ratio anomalies. Furthermore, based on the movement of stars relative to the lensed images, the microlensing signal should be time-variable. However, radio monitoring of B0128+437 by Koopmans et al. (2003) has shown a nearly time-independent flux ratio. Finally, microlensing cannot explain the observed astrometric anomalies. Thus, it would be difficult for microlensing alone to fully account for the observed properties of B0128+437.

4.2.4. Multiple Processes

After comparing our data to the existing radio data, we find that no single phenomenon seems to completely explain the unusual appearance of B0128+437. However, since each process is able to explain some aspect of the anomaly, the full effect is likely due to a combination of these mechanisms. Considering the probable late-type morphology of the lensing galaxy, this multi-process scenario could, for example, be the result of a spiral arm. The overdensity of an arm positioned near image B could be sufficient to cause the astrometric anomaly (Mao & Schneider 1998), and a GMC that is associated with the enhanced star formation in the spiral arm could produce the wavelength-dependent flux-ratio anomaly.

However, additional data and modeling are needed before a definitive explanation for the observed properties of this system can be made. Obtaining high-resolution, multi-band imaging in the optical regime will allow for better constraints on extinction. Rest-frame U- and B-band data may also provide visual confirmation of spiral arms, though given the faintness of the source, deep imaging using either AO or the JWST will be required to resolve these features. Similarly, multi-frequency radio observations can be used to probe scintillation effects such as scatter-broadening. Higher-resolution spec-

troscopy will also be useful. For example, if the single emission line associated with the lens is [O II], giving $z_l = 1.145$, then moderate-resolution spectroscopy should split the doublet and allow an unambiguous line identification to be made. Finally, grid-based modeling of the resolved Einstein ring flux may provide more robust limits on substructure (Vegetti & Koopmans 2009), allowing us to better quantify the effects of mass perturbations in this system.

5. CONCLUSIONS

We use the Keck NIRC2 plus LGS AO to observe the gravitational lens system B0128+437, and we are able to confirm the presence of the lensing galaxy and clearly separate the lensing galaxy flux from the source galaxy flux for the first time. We take advantage of the high-quality AO imaging to present new science results for the B0128+437 lens system. These results can be summarized as follows:

- For the most probable redshift $z_l = 1.145$, we measure a total K-band luminosity $\log_{10}(L_K) = (11.07 \pm 0.05) h_{70}^{-2} L_{\odot}$, an aperture luminosity within the Einstein ring radius $\log_{10}(L_{K,\text{Ein}}) = (10.61 \pm 0.05) h_{70}^{-2} L_{\odot}$, and a K-band M/L ratio $M/L_{K,\text{Ein}} = (0.68 \pm 0.05) h_{70} M_{\odot}/L_{\odot}$ for the lensing galaxy.
- We measure Kp flux ratios of $f_B/f_A = 0.17 \pm 0.03$, $f_C/f_A = 0.42 \pm 0.01$, and $f_D/f_A = 0.30 \pm 0.03$. The f_B/f_A value in the near-IR is significantly smaller than both its expected value $f_B/f_A \sim 1$ and its measured radio values. This could be due to the presence of massive substructure, propagation effects, or extragalactic microlensing. We find that none of these scenarios alone seems able to fully explain all aspects of the anomaly, implying that multiple phenomena are responsible.
- We find that there is no evidence for luminous substructure above a point-source limiting magnitude $K_p = 25.5$, corresponding to $M_V = -17$ in the B0128+437 field.

Looking at the wealth of new information obtained from B0128+437, it is clear that AO imaging is an important technique for studying gravitational lenses in new ways. With future surveys such as the Joint Dark Energy Mission (JDEM) and Large Synoptic Survey Telescope (LSST) expected to find ~ 10000 lenses (Marshall et al. 2005), of which an estimated 10% will be of the small-separation, low-mass lensing galaxy variety (Turner et al. 1984; Orban de Xivry & Marshall 2009), AO imaging of lenses will also play an important role in analyzing a large subset of future data.

We thank Aaron Dutton for helpful discussions regarding AO observing and NIRC2 data reduction and Leon Koopmans, John McKean, Phil Marshall, and Simona Vegetti for useful discussions. DJL, CDF, and MWA acknowledge support from NSF-AST-0909119. The data

presented herein were obtained at the W. M. Keck Observatory, which is operated as a scientific partnership among the California Institute of Technology, the University of California, and the National Aeronautics and Space Administration. The Observatory was made possible by the generous financial support of the W. M. Keck Foundation. The authors wish to recognize and acknowledge the very significant cultural role and reverence that the summit of Mauna Kea has always had within the indigenous Hawaiian community. We are most fortunate to have the opportunity to conduct observations from this mountain.

REFERENCES

- Auger, M. W., Fassnacht, C. D., Wong, K. C., Thompson, D., Matthews, K., & Soifer, B. T. 2008, *ApJ*, 673, 778
- Auger, M. W., Treu, T., Bolton, A. S., Gavazzi, R., Koopmans, L. V. E., Marshall, P. J., Bundy, K., & Moustakas, L. A. 2009, *ApJ*, 705, 1099
- Bertin, E., & Arnouts, S. 1996, *A&AS*, 117, 393
- Biggs, A. D. 2004, *European VLBI Network on New Developments in VLBI Science and Technology*, 163
- Biggs, A. D., Browne, I. W. A., Jackson, N. J., York, T., Norbury, M. A., McKean, J. P., & Phillips, P. M. 2004, *MNRAS*, 350, 949
- Browne, I. W. A., et al. 2003, *MNRAS*, 341, 13
- Calzetti, D., Armus, L., Bohlin, R. C., Kinney, A. L., Koornneef, J., & Storchi-Bergmann, T. 2000, *ApJ*, 533, 682
- Cambresy, L. 1999, *A&A*, 345, 965
- Crampton, D., Schechter, P. L., & Beuzit, J.-L. 1998, *AJ*, 115, 1383
- Dalal, N., & Kochanek, C. S. 2002, *ApJ*, 572, 25
- Diemand, J., Kuhlen, M., Madau, P., Zemp, M., Moore, B., Potter, D., & Stadel, J. 2008, *Nature*, 454, 735
- Fassnacht, C. D., Xanthopoulos, E., Koopmans, L. V. E., & Rusin, D. 2002, *ApJ*, 581, 823
- Fruchter, A. S., & Hook, R. N. 2002, *PASP*, 114, 144
- Grundahl, F., & Hjorth, J. 1995, *MNRAS*, 275, L67
- Keeton, C. R., Gaudi, B. S., & Petters, A. O. 2005, *ApJ*, 635, 35
- Koopmans, L. V. E., & de Bruyn, A. G. 2000, *A&A*, 358, 793
- Koopmans, L. V. E., et al. 2003, *ApJ*, 595, 712
- Mao, S., & Schneider, P. 1998, *MNRAS*, 295, 587
- Maraston, C. 2005, *MNRAS*, 362, 799
- Marshall, P., Blandford, R., & Sako, M. 2005, *New Astronomy Review*, 49, 387
- Marshall, P. J., et al. 2007, *ApJ*, 671, 1196
- McKean, J. P., Koopmans, L. V. E., Browne, I. W. A., Fassnacht, C. D., Blandford, R. D., Lubin, L. M., & Readhead, A. C. S. 2004, *MNRAS*, 350, 167
- McKean, J. P., et al. 2007, *MNRAS*, 378, 109
- More, A., McKean, J. P., More, S., Porcas, R. W., Koopmans, L. V. E., & Garrett, M. A. 2009, *MNRAS*, 394, 174
- Myers, S. T., et al. 2003, *MNRAS*, 341, 1
- Orban de Xivry, G., & Marshall, P. 2009, *MNRAS*, 399, 2
- Phillips, P. M., et al. 2000, *MNRAS*, 319, L7
- Ros, E., Guirado, J. C., Marcaide, J. M., Pérez-Torres, M. A., Falco, E. E., Muñoz, J. A., Alberdi, A., & Lara, L. 2000, *A&A*, 362, 845
- Sérsic, J. L. 1963, *Boletín de la Asociación Argentina de Astronomía La Plata Argentina*, 6, 41
- Springel, V., et al. 2008, *MNRAS*, 391, 1685
- Tortora, C., Napolitano, N. R., Romanowsky, A. J., Capaccioli, M., & Covone, G. 2009, *MNRAS*, 396, 1132
- Turner, E. L., Ostriker, J. P., & Gott, J. R., III 1984, *ApJ*, 284, 1
- Vegetti, S., & Koopmans, L. V. E. 2009, *MNRAS*, 392, 945
- Wambsganss, J. 2006, *Gravitational Lensing: Strong, Weak and Micro*, Saas-Fee Advanced Courses, Volume 33. ISBN 978-3-540-30309-1. Springer-Verlag Berlin Heidelberg, 2006, p. 453, 453
- Xu, D. D., et al. 2009, *MNRAS*, 398, 1235
- Zeiger, B., & Darling, J. 2010, *ApJ*, 709, 386